Scripta Materialia xxx (2015) xxx–xxx

Contents lists available at ScienceDirect

Scripta Materialia

journal homepage: www.elsevier.com/locate/scriptamat

Viewpoint Paper

Thermoelectric topping cycles with scalable design and temperature dependent material properties

Kazuaki Yazawa *, Ali Shakouri

Birck Nanotechnology Center, Purdue University, 1205 W State Street, West Lafayette, IN 47907, USA

ARTICLE INFO

Article history:
Received 2 March 2015
Revised 11 May 2015
Accepted 17 May 2015
Available online xxxx

Keywords:
Thermoelectric materials
High temperature
Topping cycle
Co-generation
Power generator

ABSTRACT

Analysis and optimization of topping thermoelectric generators with bottoming Rankine cycle is presented. Interface temperature between the two cycles is optimized for fuel efficiency. It is shown that the topping thermoelectric generator may increase the system efficiency by 6% for a coal-fired power plant with approximately 0.2–0.3 $/W in material cost. The topping cycle can be a viable large scale application of thermoelectric generators since peak ZT of the material can be optimized in a narrow temperature range without cascading.

1. Introduction

It is remarkable that, since 1961 [1], a very early success of the thermoelectric (TE) power generator was a high temperature (~1000 °C) application enabling spacecraft powering systems by an auxiliary nuclear reaction heat source called the radioisotope thermoelectric generator (RTG). The RTG materials first used lead telluride (PbTe) and later switched to silicon germanium (SiGe). On the other side of the extreme temperature, the success of multistage thermoelectric coolers in refrigeration (~−140 °C in vacuum) [2] has been well known. These historical facts show that thermoelectric power generators are scalable in a wide range of temperatures.

In industrial power generation, coal fired midscale power plants have provided 50.4% of the electricity supply in the U.S. [3]. Natural gas is typically used for micro-grids or on-site power generation, while the penetration of renewable energy sources remains a much lower fraction. Renewable resources are hindered by capital cost, intermittency, and seasonal swings [4,5]. The energy conversion efficiency of Rankine cycle technology alone is around 40%, which has a reasonable economic return on investment. However, higher efficiency is also critical for conserving natural resources [6] as well as for the reduction of CO_2 equivalent gas emissions in preventing global warming. The physics behind the proposed approach is based on maximizing exergy (useful energy) in a large temperature gap between the fuel burning temperature and the gas temperature coming into the turbine. A state-of-the-art combined Brayton–Rankine cycle uses a wider temperature span and generates power with more than 55% efficiency. However, the gas turbine system is significantly complex and impacted by surface to volume ratio; hence, the system will not be scalable to smaller than 100s MW power plants.

Thermoelectric generation is highly scalable by arraying solid-state modules to cover any size heat source and generate power from 1 W to more than 100s MW. These are very favorable features mitigating the higher side of the unused temperature in fuel burning power generation systems. In a previous work, we investigated the TE topping cycle with the Rankine cycle [7]. Fig. 1 demonstrates the system performance with the topping TE and indicates an optimum steam temperature for maximizing total output power. Another team investigated the TE topping Brayton cycle [8], but here we focus more on the smaller scale power plants that are desirable for distributed and smart grid application.

One can increase the total efficiency even further by utilizing TE for waste heat recovery [9,10] from exhaust gas that comes from internal combustion engines, etc. The waste heat recovery can coexist with the topping cycle without interference. We will compare these in performance and cost effectiveness.

Fig. 2 illustrates the system schematic of a current state-of-the-art 520 MW class power plant unit [11]. To enable a realistic and practical evaluation, Silaen et al. [12] analyzed the fluid-dynamic behavior of the gas in the furnace and solved the conjugate heat transport using computational thermo-fluid

* Corresponding author.
E-mail address: kyazawa@purdue.edu (K. Yazawa).

http://dx.doi.org/10.1016/j.scriptamat.2015.05.037
1359-6462/

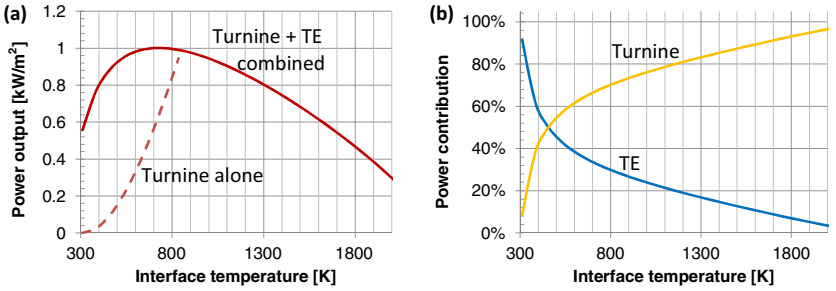

Fig. 1. (a) Power output of the combined system as a function of the interface temperature with broken curve shows the turbine only power output with is limited by the steam temperature below ~800 K for cost effective applications, (b) TE and steam turbine contributions for the system power output. TE module assumes a constant figure-of-merit $Z = 6.67e{-}4$ for the entire temperature range of investigation, and the TE modules are designed to be optimized for maximum power output. The interface temperature assumes the steam temperature at boiler for a steam turbine (Rankine cycle).

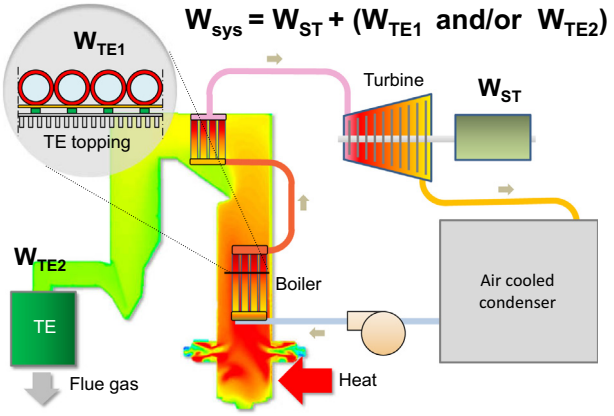

Fig. 2. System diagram of TE topping cycle W_{TE1} and flue gas W_{TE2} power generators with a Rankine cycle coal-fired power plant W_{ST} with air cooled condenser. Overall power output is W_{sys} depending on whether the topping cycle or flue gas TE power generator is integrated, or both.

dynamic analysis. With surface area enhancement, the TE modules are designed between the wall of the boiler and the steam tubes. The TE elements are optimized locally for the simulated gas temperature profile, which is graded along the wall height of over 20 m. These basic designs and analyses enable the prediction of a realistic overall efficiency in accordance with temperature–entropy (T–s) diagram analysis for a complete superheated Rankine cycle.

Considering the scalability of TE in design for temperature and power range, we investigate and optimize the TE generator design for the system efficiency and cost performance in the above specific case of a power plant while considering a constant ZT value as a universal number. Then, we discuss the impact of the real material, which has temperature dependency for three thermoelectric properties.

2. Materials for high temperatures

RTGs typically use silicon germanium (SiGe) alloys. The system-level conversion efficiency for state-of-the-art RTGs is about 6%, with lifetimes in excess of 30 years [1]. We base our analysis on well characterized SiGe material [13,14]. The SiGe used for spacecraft applications can be improved, and its figure-of-merit (ZT) has been increased to ZT = 1 via nanostructuring, which decreases thermal conductivity without substantially changing the electrical properties [15]. Germanium, however, is a less abundant material and is unfortunately not practical for large-scale deployment in power plant applications. The use of SiGe will also slightly limit the highest operating temperature at the hot side of the TE leg. State-of-the-art p-type $Yb_{14}MnSb_{11}$ and n-type $La_{3-x}Te_4$ have demonstrated maximum ZTs in the range of 1.2–1.5 at 1300 K and are being actively pursued by NASA JPL for space applications, but these are not abundant either. If we traded off the performance, nanostructured silicon materials could be considered as they have reasonable ZTs (0.3–0.4) at high temperatures. Given the variability in ZT values as well as the practical material considerations, we use ZT as an adjustable parameter within the practical range described above.

We subsequently investigate the design of the thermoelectric module and the potential parasitic losses. Based on preliminary calculations presented in Ref. [16], the optimum TE leg thickness for the particular boiler described in Section 2 should be approximately 1.3 mm considering the currently available SiGe with 10% fractional area coverage of TE legs inside the module. This will require a metal/semiconductor contact resistivity in the range of 10^{-5} Ω-cm^2, which has been achieved [17]. Also, thermal parasitic losses need to be considered through the non thermoelement areas via radiation heat transfer and gap material (usually air) heat conduction. Based on Ref. [17], these parasitic losses are less than 10% of the heat conduction through the thermoelement with 10% fractional area coverage. If needed, a partial vacuum ranging 500 Pa or a coating with reduced emissivity by 0.3 may cut down on the loss contribution by less than 2% for each.

3. Optimization of TE design

A typical TE generator consists of n-type and p-type semiconducting materials connected together in series and placed in parallel along the heat flow direction. At the junctions of n- and p-type materials, electronic potential is created in proportion to the temperature difference; hence, an electric current is generated as the circuit closes and eventually generates power at the external load. The power generation is measured by three key properties: Seebeck coefficient (S) [V/K], thermal conductivity (β) [W/mK], and electrical conductivity (σ) [1/Ωm]. The well-known dimensionless figure-of-merit of TE material ZT is defined by

$$\mathrm{ZT} = \left(\frac{\sigma S^2}{\beta}\right) T \qquad (1)$$

where, T is the absolute mean temperature of the TE element.

A TE power generation system can be modeled based on a generic thermal equivalent circuit taking into account external finite thermal resistances with the hot and cold reservoirs, as shown in Fig. 3. We introduce a fill factor F, which is the fractional area coverage of a thermoelement per unit substrate area. Due to the abrupt cross sectional area change in heat current flow, it introduces three-dimensional spreading or constriction thermal

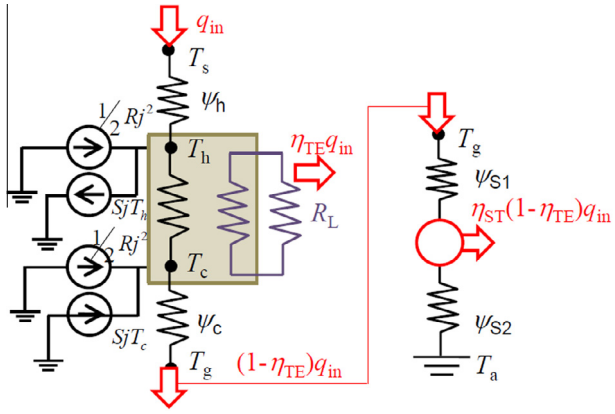

Fig. 3. Thermal network model. The left hand side flow shows the TE topping cycle, while the right hand side shows the bottoming Rankine cycle. T_s is the coal burning gas temperature and T_a is the ambient air temperature for air cooling condenser system.

resistances. Under temperature gradients, electric potential generated in the thermoelement induces electric current flow when an external electrical load is connected to the electrodes. This load should be optimized in order to extract the maximum power output or the highest energy conversion efficiency. In this study, the power output is considered per unit area of heat flow.

Solving the set of energy balance equations at each temperature node, the power output per unit area w [W/m^2] is given by Eq. (2)

$$w = \left(I^2 mR\right)\Big/A = \frac{mZ}{(1+m)^2}\frac{\beta F}{d}(T_h - T_c)^2 \tag{2}$$

where I is the induced current, A is the substrate area, R is the internal resistance, m is the load resistance ratio ($R_{load} = mR$), T_h is the hot side leg temperature, and T_c is the cold side leg temperature. To consider the influence of external thermal resistances, the equation for power output is transformed as in Eq. (3).

$$w = \frac{mZ}{(1+m)^2}\frac{d\beta F}{(d+\beta FA\sum \Psi\kappa)^2}(T_s - T_g)^2 \tag{3}$$

where $\Sigma\Psi$ is the sum of the external thermal resistances, including heat sinks and spreading thermal resistances in thermoelectric module plates, T_s is the heat source temperature, T_a is the ambient temperature, and κ is a dimensionless factor as found in Eq. (4).

$$\kappa = \left(1 + \frac{Z}{2(1+m)^2}((2m+1)T_h + T_c)\right)\frac{\Psi_h}{\sum\Psi} + \left(1 + \frac{Z}{2(1+m)^2}(T_h + (2m+1)T_c)\right)\frac{\Psi_c}{\sum\Psi} \tag{4}$$

To obtain the maximum w, co-optimizing the factors m and d by taking the derivative of w to be zero, the optimum leg length d_{opt} is found as

$$d_{opt} = \kappa\beta FA\sum\Psi \tag{5}$$

κ is found here as the ratio of the internal leg thermal resistance to the sum of the external thermal resistances, only at the optimum w. However, κ must include the electrical resistance ratio m, due to the characteristics of thermoelectric. Also, Eq. (4) shows that this ratio depends on the ratio of asymmetric external thermal resistances (Ψ_c/Ψ_h).

By electro-thermal optimization, the maximum output power is found at a single point with electrical impedance match m exactly the same as in the conventional expression

$$m = \sqrt{1+ZT} \tag{6}$$

while, κ maintains a similar value to m and only in the special case $\Psi_c = \Psi_h$, κ equals m. In this symmetric thermal resistance system, the maximum power output becomes simpler as

$$w_{max} = \frac{Z}{4(1+m)^2}\frac{1}{A\sum\Psi}(T_s - T_g)^2 \tag{7}$$

The important fact here is that the fill factor proportionally changes the optimum leg length, but does not obviously impact the power output. In some case studies [18,19], a fill factor of more than 10% affects the power output much less than 1%, while a fill factor of 10% reduces the optimum thickness by 10% and the cross section area by 10%. Therefore, the volume reduction by a smaller fill factor has a significant impact on cost per performance. In a further analysis, we showed that thermal conductivity is the only material property that impacts the cost performance linearly in the maximum power output design [20]. This is substantiated by Eq. (5). While power output is the same as long as Z value is fixed, reducing thermal conductivity will reduce the amount of required TE material for a given external reservoir thermal resistances.

4. Cost-performance analysis

Fig. 4 shows the net TE power output (payback power) per unit area considering the pump power consumption for the refrigerant, i.e. air or water, at the maximum power output design. The left side plot shows the air cooling range up to a heat flux of 10^{+5} W/m^2 and the right side shows the range of water cooling up to a heat flux of 10^{+6} W/m^2. The power required for pumping is also plotted, which increases more rapidly as a function of heat flux compared to the TE power output. Although the thermoelectric power generation efficiency is in the 5–11% range, the power output per unit area is much larger than that of photovoltaic solar cells in the 10–20% range because of the high heat flux densities available.

Fig. 5 shows a more specific and comprehensive analysis of the topping TE generator and waste heat recovery (WHR) TE generator for the 520 MW class coal fired power plant described earlier. A thermoelectric module with a smaller fill factor requires a significantly lower initial cost to build. The material cost is proportional to F^2 and will be negligible even considering the use of a relatively expensive thermoelectric material. The cost of the thermoelectric material, SiGe, for the topping cycle is controlled by the market price of germanium ~$2000/kg. For the WHR, the cost of the PbTe material is $500/kg and is assumed based on industrial input.

For example, to replace the current cooling tower condensers with air cooled condenser (ACC) units to save fresh water, the initial cost increases by $79.5 M for a 500 MW class power plant. Based on $0.05/kWh for the baseline electricity price and 30 years of operation, this initial cost is only ~1% of the overall system investment.

In the power plant, the thermoelectric is placed in the boiler in between the furnace gas and the steam tubes, with the interim wall plate facing the furnace. The effective heat transfer coefficient for the hot side wall is 246 [W/m^{2}K] and the cold side is 722 [W/m^{2}K]. Due to the increased thermal resistance, by inserting thermoelectric, the hot side heat transfer needs to be enhanced by surface area extension through fin surface or by increasing the hot gas flow speed through changing the burner design. By optimization of the thermoelectric element design, the temperature at the hot side T_h = 1170 °C and the cold side T_c = 742 °C at the maximum design point are found, respectively, while the gas temperature T_s is 1407 °C and the steam temperature T_g is 374 °C, see Ref. [12].

The cost details of the TE generators are shown in Table 1 followed by an overall performance and cost comparison shown in

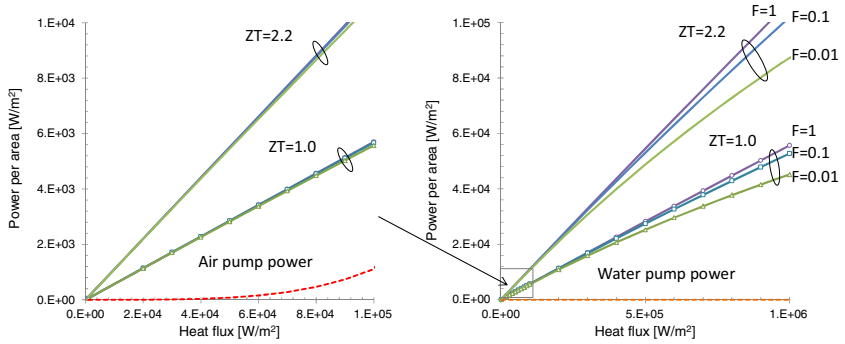

Fig. 4. Power output per unit area and pump power consumption in the maximum power output design: T_s = 600 K, T_a = 300 K, ZT = 1 with β = 1.5 W/mK and ZT = 2.2 with β = 1.01 W/mK, air fan efficiency of 30%, water heat sink pump efficiency of 60% with variations of fill factor F = 0.01, 0.1 and 1. The thermal conductivity of the TE substrate is 100 W/mK with 0.4 mm thickness for both sides, and the thermal interface resistances for contacts are included in the external thermal resistances. The efficiency for ZT = 1 and 2.2 is found to be 5.7% and 11.0%, respectively.

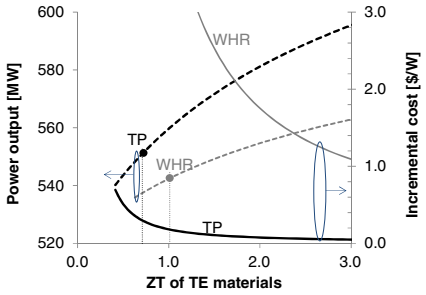

Fig. 5. Power output and incremental cost as functions of average ZT of thermoelectric material for the cases of topping cycle (TP) and waste heat recovery (WHR). ZT ~ 0.7 with nanostructured SiGe for TP and ZT ~ 1.0 with advanced PbTe for WHR, respectively, are used as the typical values.

Table 1
Details of TE topping generator with 31.0 MW_e output.

Elements	Material	Material price	Dimensions	Mass
Thermoelectric (TE)	SiGe	US$2000/kg	F = 10%, t = 1.3 mm	4.3 ton
High temperature heat fins, substrate for TE elements	Mo	US$20/kg	Area 8541 m^2, t = 0.2 mm & fins	35.1 ton
Surface coating	Al_2O_3/TiO_2	US$2/kg	t = 20 μm	675 kg

Table 2
Details of the TE waste heat recovery with 22.4 MW_e output.

Elements	Material	Material price	Dimensions	Mass (ton)
Thermoelectric (TE)	PbTe	US$500/kg	F = 10%, t = 2.9 mm	197
High temperature heat fins, substrate for TE elements	Al_2O_3	US$2/kg	Area 82,745 m^2, t = 0.2 mm	131

Note: F stands for fractional area ratio and t stands for thickness.

Table 2. If the TE generator for waste heat recovery uses 100% of the available heat in the flue gas discharged, it occupies almost 10 times the area compared to the topping TE in the boiler section. The additional investment for waste heat recovery shows an order of magnitude larger than that of the topping cycle. This is due to the lower heat fluxes available at the bottoming cycle. Fig. 5 shows the power output and the incremental investment cost as the function of the average ZT of the material. The graph shows the future potential of the TE generators when the thermoelectric material properties are improved. The ZT has a significant role in the investment cost. However, the waste heat recovery still costs much more than the topping cycle (see Fig. 5).

5. Thermo-mechanical concern

A large temperature difference between the hot and the cold substrates in the TE modules could result in large local thermo-mechanical stresses and possible mechanical failure. The thermo-mechanical expansion concern also contradicts the thermodynamic benefit. Analytic modeling has been conducted [21] in previous work, and we showed that the small fill factor does not necessarily push the local mechanical stress at the contacts more (see Fig. 6). Rather, the corner legs of the large number of arrays may pose a much harder challenge and risk for reliability [22].

The above analysis and the numerical modeling [23] show that the maximum share stress at solder joint is $\tau_{max}(F = 10\%) < \tau_{max}(F = 50\%)$. In analytic modeling, decreasing the fill factor from 25% to 3% reduces the maximum shear stress by less than half. This is in agreement with the results obtained by the 3D finite element analysis of a 2-leg TEM structure assuming homogenous CTE in all of the layers. Imposing structural boundary conditions on either the hot or the cold side of the structure does not change the predicted trend. However, this constraint leads to generation of a stronger shear stress in the contact near the constrained side compared to in the free-standing case. Modules with multiple legs produce different results compared to the above simple two leg design. A CTE mismatch between the layers could produce significant local shear stress at a high temperature. This local stress should be proportional to $\Delta\alpha\Delta T$. This effect could be mitigated by changing the geometry or choosing material properties that are closely matched.

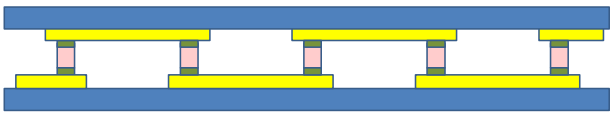

Fig. 6. Diagram of the TE module structure for stress analysis. The thin and small center legs (pink) are the thermoelectric materials and the green contacts are the solder joints, which are connected by a metal layer (yellow) layout on the outside insulator substrates (blue). (For interpretation of the references to color in this figure legend, the reader is referred to the web version of this article.)

6. Environmental impacts

In 2013, 16.5 QUADS of coal was used for power generation. If the present TE topping technology is applied to 5% of the currently working power plants with increasing 6% efficiency, the overall primary energy saving will be 1.45×10^7 MWh (522×10^8 MJ) per year, which is equivalent to reducing CO_2 emissions by 4.7 million ton-CO_2 per year just in the U.S. The above implementation is equivalent to 1660 MW power generation from the thermoelectric topping cycle, and it will require approximately 230 tons of SiGe material [24]. If the material is realized by a ratio Si/Ge to be 80/20 through utilizing nanostructure for appropriate ZT, 46 tons of purified germanium will be required. On the other hand, the domestic reserve of germanium in the U.S. is estimated to be only 400 tons, according to a government report [25]. Although this reserve amount will cover the required germanium amount, 12% of the reserve is a significant volume to consume and so the development of an alternative high temperature material must be seriously considered.

According to the phase diagram of $Ge_{1-x}Si_x$ system [26], the phase transition temperature is greater for higher silicon content materials. Even though it is a big advantage to contain a certain ratio of germanium for performance, a material nearly silicon ($x \sim 1$) is desired because of the temperature tolerance, cost, and conservation of natural resources. The n-type [27] and n-type [28] bulk alloys of approximately 80/20 blend of Si/Ge thermoelectric materials with nanostructures have been developed and the performance has been found to be near $ZT \sim 1$ at near 1000 K condition. Si nanowires have been studied quite a lot due to the significant thermal conductivity reduction from their confined geometry with a large power factor. Although most of the experimental research has been carried out at near room temperature, e.g. [29–31], a potential of high performance at an elevated temperature is expected. A bulk-like nanostructured silicon at elevated temperature 1275 K was investigated and it was reported that $ZT \sim 0.7$ [32]. This team also reported the performance of a very low germanium content 2.5% Ge nanostructured bulk Si_xGe_{1-x} that shows approximately $ZT \sim 0.7$ for n-type and $ZT \sim 0.2$–0.4 for p-type at 1275 K as well.

For another potential candidate for an alternate material, the Jet Propulsion Laboratory (JPL) has been pursuing the development of high-efficiency TE materials and segmented unicouples for integration into an advanced radio isotope generator (RTG). The high-temperature segments of these unicouples are composed of p-type $Yb_{14}MnSb_{11}$ and n-type $La_{3-x}Te_4$. The lower segments are made of skutterudite materials for this study. These materials are capable of sustained operation at temperatures up to 1273 K and have been extensively developed at JPL. Aging studies have been conducted for $Yb_{14}MnSb_{11}$ and n-type $La_{3-x}Te_4$ materials and the materials and their TE properties have been demonstrated to be stable at temperatures up to 1323 K for up to 24 months. These materials have at least a ten times larger reserve compared to germanium but still contain the rare metals, so the cost issue may remain.

7. Temperature dependent ZT properties

The temperature dependency of TE material properties is a well-known characteristic and it has become a significant concern as the temperature range of the power generator gets larger. The three component properties for the figure-of-merit ZT value have individual temperature dependencies and are linked to each other. The general trend of the properties, thermal conductivity, electrical conductivity, and Seebeck coefficient as a function of carrier concentration is explained in [33]. Temperature dependency occurs

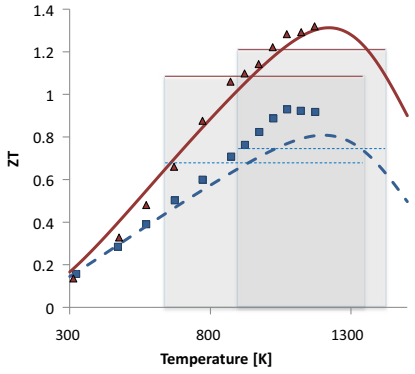

Fig. 7. Temperature dependent ZT value of n-type by Wang et al. [27] (square dot) and p-type by Joshi et al. [28] (triangle dot) with predicted curves with using open access Boltzmann solver developed by Je-Hyeong Bahk et al. [34]. The taller box shows the temperature band (905–1422 K) of the topping cycle with the mean ZT values 0.75 and 1.21 for n-type and p-type, respectively. The lower box shows the full temperature band (645–1335 K) assuming a cold reservoir temperature 300 K with the mean ZT values 0.68 and 1.08 for n-type and p-type, respectively. Both use the heat source temperature 1680 K.

for all three parameters. The thermal conductivity of the semiconductors is generally reduced as the temperature increases. However, major carrier contribution in heat transport increases with the increasing temperature. Eventually, the effective thermal conductivity increases at a high temperature due to bipolar thermal conduction. The electrical conductivity first decreases due to increased scattering but eventually increases due to the generation of free electrons/holes at very high temperatures. In contrast, the absolute value of the Seebeck coefficient increases as the temperature increases and then reduces sharply at high temperatures due to the bipolar conduction. Hence, most of the thermoelectric materials have a strong temperature dependent ZT and an optimum temperature for the maximum ZT value.

The following figure (Fig. 7) shows an example of $Si_{0.8}Ge_{0.2}$ nano inclusion material. Depending on the temperature range, the mean ZT value changes significantly. To find a more accurate prediction of the performance, we have to discretize the temperature band and optimize the local performance across the whole temperature range.

Taking advantage of the topping cycle, one can optimize the peak ZT of the material in a narrow temperature range without the need to cascading.

8. Conclusions

We investigated the high temperature topping cycle to harvest unused exergy in a coal fired power plant. We analyzed the performance of TE generators designed with an existing 520 MW class Rankine cycle power plant. The TE topping cycle increases the system efficiency by 6% of the overall system with a ZT value 0.7 of SiGe based nanomaterial. The additional implementation cost of 0.3 $/W could be possible even using an expensive raw material SiGe ~2000 $/kg since a smaller fill factor ~10% requires a significantly small volume of such exotic materials. The topping cycle provides nearly an order of magnitude cost effective power generation compared to the waste heat recovery from flue gas discharged in the same power plant. Even if 5% of the current coal fired power plants implement this technology, the positive potential environmental impact is estimated to save 4.7 million ton-CO_2 per year. On the other hand, however, consumption of germanium will be a significant challenge in saving rare material natural resources. Development of alternative thermoelectric materials for high temperature application needs to be explored.

Please cite this article in press as: K. Yazawa, A. Shakouri, Scripta Mater. (2015), http://dx.doi.org/10.1016/j.scriptamat.2015.05.037

The key findings for the thermoelectric material properties in cost effective power generations are that (1) reduction of thermal conductivity is the most desired approach for cost effective power generation. As far as the ZT value remains, the power generation performance remains the same while the lower thermal conductivity reduces the material volume, and that (2) due to the temperature dependence of the thermoelectric material properties, the peak ZT is not the most important parameter. Instead, the mean ZT across the temperature range will be a reasonable index of performance. Engineering materials with temperature dependent ZT with a wide plateau is another direction for materials R&D.

Acknowledgments

The authors would like to thank Prof. Timothy S. Fisher, Prof. Chenn Qian Zhou, and their students and postdocs for helping with the analysis by providing a useful discussion on high temperature interfaces and materials data as well as power plant technical information and computational thermo-fluid dynamic analysis on boilers. We would also like to thank Dr. Je-Hyeong for providing the material ZT analysis using the Boltzmann transport equation. Lastly, the authors acknowledge the support from the Center for Energy Efficient Materials funded by the Office of Basic Energy Sciences of the U.S. Department of Energy.

References

[1] G.L. Bennet, in: D.M. Rowe (Ed.), CRC Handbook of Thermoelectrics, CRC Press, 1995, pp. 515–537.
[2] R. Marlow, E. Burke, in: D.M. Rowe (Ed.), CRC Handbook of Thermoelectrics, CRC Press, 1995, pp. 597–607.
[3] U.S. Energy Information AdministrationElectric Power Monthly with Data for August 2013, U.S. Department of Energy, 2013.
[4] A. Zahedi, Renew. Sustain. Energy Rev. 15 (1) (2011) 866–870.
[5] D.L. King, W.E. Boyson, J.A. Kratochvil, in: Proc. 12th IEEE Photovoltaic Specialists Conf., 2002, pp. 1356–1361.
[6] Electric Power Research Institute, Program on Technology Innovation: New Concepts of Water Conservation Cooling and Water Treatment Technologies, 2012, p. 1025642.
[7] K. Yazawa, A. Shakouri, Appl. Energy 109 (2013) 1–9.
[8] C.B. Knowles, H. Lee, J. Appl. Phys. 112 (2013) 073515.
[9] L.E. Bell, Science 321 (5895) (2008) 1457–1461.
[10] J. Yang, F.R. Stabler, J. Electron. Mater. 38 (7) (2009) 1245–1251.
[11] K. Yazawa, Y.R. Koh, A. Shakouri, in: Proc. ASME InterPACK2013, 2013, InterPACK2013-73195.
[12] A. Silaen, B. Wu, D. Fu, C. Zhou, K. Yazawa, A. Shakouri, in: Proc. ASME 4th Micro/Nanoscale Heat & Mass Transfer International Conf., 2013, MNHMT2013-22248.
[13] A. Shakouri, Proc. IEEE 94 (8) (2006) 1613–1638.
[14] C.B. Vining, in: D.M. Rowe (Ed.), CRC Handbook of Thermoelectrics, CRC Press, 1995, pp. 329–337.
[15] N. Mingo, D. Hauser, N.P. Kobayashi, M. Plissonnier, A. Shakouri, Nano Lett. 9 (2) (2009) 711–715.
[16] K. Yazawa, A. Shakouri, J. Appl. Phys. 111 (2012) 024509.
[17] O.J. Mengali, M.R. Seiler, Adv. Energy Convers. 2 (1962) 59–68.
[18] K. Yazawa, A. Shakouri, Environ. Sci. Technol. 45 (17) (2011) 7548–7553.
[19] K. Yazawa, A. Shakouri, in: Proc. MRS 2011fall Meeting, Symposium O, 2011.
[20] K. Yazawa, A. Shakouri, J. Mater. Res. 27 (09) (2012) 1211–1217.
[21] E. Suhir, A. Shakouri, ASME J. Appl. Mech. 79 (6) (2012) 061010.
[22] E. Suhir, A. Shakouri, ASME J. Appl. Mech. 80 (2) (2013) 021012.
[23] A. Ziabari, K. Yazawa, A. Shakouri, in: Proc. 32nd ITCC and 20th ITES, 2014.
[24] K. Yazawa, M. Hao, B. Wu, A.K. Silaen, C.Q. Zhou, T.S. Fisher, A. Shakouri, Energy Convers. Manage. (2014).
[25] U.S. Geological Survey Minerals Yearbook 31 Germanium, 2013.
[26] R.W. Olesinski, J.C. Abbaschian, The Ge–Si (Germanium–Silicon) System, Bulletin of Alloy Phase Diagrams 5, ASM publication, 1984. pp. 180–183.
[27] X.W. Wang, H. Lee, Y.C. Lan, G.H. Zhu, G. Joshi, D.Z. Wang, J. Yang, A.J. Muto, M.Y. Tang, J. Klatsky, S. Song, M.S. Dresselhaus, G. Chen, Z.F. Ren, Appl. Phys. Lett. 93 (2008) 193121.
[28] G. Joshi, H. Lee, Y. Lan, X. Wang, G. Zhu, D. Wang, R.W. Gould, D.C. Cuff, M.Y. Tang, M.S. Dresselhaus, G. Chenand, Z. Ren, Nano Lett. 8 (12) (2008) 4670–4674.
[29] A.I. Hochbaum, R. Chen, R.D. Delgado, W. Liang, E.C. Garnett, M. Najarian, A. Majumdar, P. Yang, Nat. Lett. 451 (2008) 163–168.
[30] B.M. Curtin, J.E. Bowers, Mater. Res. Soc. Symp. Proc. 1408 (2012).
[31] D. Dávila, A. Tarancón, M. Fernández-Regúlez, C. Calaza, M. Salleras, A. San Paulo, L. Fonseca, J. Micromech. Microeng. 21 (10) (2011) 104007.
[32] S. Bux, J.-P. Fleurial, R. Blair, P. Gogna, T. Caillat, R. Kaner, Mater. Res. Soc. Symp. Proc. 1166 (2009). 1166-N02-04.
[33] D.M. Rowe, in: D.M. Rowe (Ed.), CRC Thermoelectrics Handbook Micro to Nano, CRC Press, 2006. pp. 1-1–1-14.
[34] J.-H. Bahk, M. Youngs, K. Yazawa, A. Shakouri, in: Proc. 43rd ASEE/IEEE Frontiers in Education Conf., 2013.